JOURNAL OF CATALYSIS 95, 71–83 (1985)

Nickel Catalyst Deactivation in the Steam-Carbon Reaction

CARL R. F. LUND

Exxon Research and Engineering Company, Corporate Research-Science Laboratory, Annandale, New Jersey 08801

Received December 21, 1984; revised March 28, 1985

Nickel deactivation during steam gasification of carbon is shown to be two types which depend upon the chemical nature of the carbon. For graphite, deactivation is moderate and may be attributed either to catalyst clustering or to effects of the carburization of the nickel. With less-ordered carbons, like Spherocarb, deactivation is severe and rapid. The catalyst particles apparently lose surface area due to encapsulation by a graphite overlayer. Dual-bed gasification indicates that the carbon substrate releases hydrocarbon species which subsequently decompose on the nickel. Analogous results are obtained during the CO_2 and H_2 gasification reactions.

INTRODUCTION

In the steam gasification of carbon, nickel is many times more active as a catalyst than potassium (*1*), whereas potassium has been identified and developed for commercial application in coal gasification (*2*). One problem encountered with nickel catalysts for steam gasification of carbon is a propensity to deactivate (*1*). The deactivation of nickel has been attributed to many causes; this study has been undertaken in order to identify the cause for nickel catalyst deactivation. The findings from this investigation may also have implications in the steam reforming area where supported nickel is most often used (*3*). Supported nickel steam reforming catalysts are often decoked in steam, and at least part of the decoking is catalyzed by the nickel (*4*).

Many researchers have examined the nickel catalyzed steam gasification of carbon. However, it is difficult to formulate a consistent model of the process because there are many forms in which carbon is found. For example, the catalytic behavior of nickel during steam gasification of petroleum coke need not be the same as that of graphite. In addition to differences in basic structure, even carbons which are structurally similar may still differ markedly with respect to the amount and types of impurities which they contain. Also, Holstein (*5*) has demonstrated that it is important to apply appropriate reactor design procedures in the analysis of the steam-carbon reaction.

The literature concerning catalyzed steam gasification of carbon is extensive, but it has been reviewed recently (*6, 7*). The dissociation of H_2O at the nickel surface has been proposed to be the rate-limiting step in the overall reaction mechanism. Thus, it has been suggested that the affinity of the catalyst for oxygen will determine the catalytic activity.

Thus deactivation of nickel has also been studied many times, but a consensus does not exist regarding the mode of catalyst deactivation. Colle *et al.* (*8, 9*) observed sintering of the dispersed nickel catalyst during gasification but found that the concomitant metal surface area decrease did not account for the lost activity. The extent of nickel reduction measured by magnetization was observed to increase as the catalytic activity decreased. Moulijn and co-workers (*1, 10, 11*) also investigated nickel deactivation during steam gasification. When the total rate was normalized using the fraction of the ultimately convertible carbon present, the resulting "rate" was constant. Deactivation was attributed to the formation of an amorphous carbon

0021-9517/85 $3.00

layer on the metal surface preventing diffusion of the carbon substrate through the metal.

McKee (*12*) reported that nickel did not show significant catalytic activity in H_2O unless H_2 was added to the feed. The H_2 was suggested to be necessary to maintain the catalyst in the metallic state. Both these interpretations appear to conflict with experimental results from other studies (*1, 8–11*). Tamai *et al.* (*13–15*) reported that the catalytic reaction proceeded through three stages: devolatization, low temperature–high activity, and high temperature–low activity. Those researchers, like many others who have studied the nickel steam gasification system, did not observe or did not examine catalyst deactivation.

METHODS

Catalyst activity was monitored in a quartz tubular reactor equipped with a basket which housed the catalyzed carbon. The basket bottom was a quartz frit, and the basket diameter was only slightly less than the reactor tube wall so that gas bypassing of the sample was minimal. The basket was supported on a movable thermocouple probe which allowed the sample to be rapidly repositioned from outside the furnace to a location within the heated zone. The reactor was supplied N_2, Ar, CO_2, CO, CH_4, and H_2 from cylinders; all gases were of better than 99.99% stated purity. Water was added by bubbling the gas through heated, distilled water; saturation of the gas was assumed. Measurements of the water content of the gas by condensation and weighing showed at least 95% saturation at all flow conditions with this particular equipment. After the reactor step the gas was dried and analyzed chromatographically for CO, CO_2, H_2, and CH_4.

In a typical gasification experiment, a measured mass of carbon/catalyst was put in the quartz sample basket while the reactor system was purged with Ar. The sample basket was then introduced, through a large compression fitting, into the bottom of the quartz reactor tube (but outside the preheated furnace zone). The argon purge was maintained throughout the loading process and for a period after loading sufficiently long to sweep out any air which entered with the sample basket. The basket was then pushed up into the furnace tube to a position where the temperature was 1000 K and held there for 5 min in 100 sccm[1] Ar; this was the standard pretreatment. If desired, the sample temperature was then changed by repositioning the sample basket. Once the temperature was stable, the feed gas was changed to the desired composition by resetting the mass flow controllers and/or passing the gas through the the saturator. After the experiment was finished the sample was removed and weighed. Thus in a typical experiment the weight change of the sample was measured as well as the dry reactor outlet gas composition at specific times into the experiment.

The catalyzed samples used in these experiments were prepared using one of two carbons. The first was SP-1 graphite purchased from Union Carbide and guaranteed to have 6 ppm total maximum spot impurities. The second carbon was Spherocarb, a carbon molecular sieve purchased from Analabs, which was assumed to behave similarly to char during nickel-catalyzed steam gasification. Spherocarb has been reported to be nearly devoid of mineral impurities (0.1% ash) but has high reported oxygen content (2.2 wt%) (*16*). The nickel catalyst was typically added to either of these carbons by dissolving in methanol an appropriate amount of $Ni(NO_3)_2 \cdot 6H_2O$ for the catalyst loading desired and adding the carbon to the solution. The solvent was then evaporated, and the sample was vacuum-dried at 373 K for ca 4 h.

In some experiments uncatalyzed carbon was used. Spherocarb, SP-1 graphite and activated coconut charcoal (Fisher Scientific) were used as received. A sample of Illinois No. 6 coal, pretreated to remove all

[1] Standard cubic centimeters per minute.

minerals except pyrite, was heated for 1 h at 1273 K in flowing Ar before use.

For electron microscopy studies, natural single-crystal graphite was cleaved and mounted on microscope grids using standard procedure (*17*). Nickel was evaporated onto the sample from a nickel wire wrapped around a tungsten filament. Evaporation was done by resistive heating of the filament in a bell jar evacuated to below 10^{-4} Pa. The amount of nickel on the sample was estimated to be one monolayer. To examine actual samples from the reactor in the scanning transmission electron microscope (STEM), the samples were ground in an agate mortar and dispersed on a holey carbon film (*18*).

The rate of low-temperature water-gas shift (LTWGS) was also used as a catalyst probe. The LTWGS rate was measured during a steam gasification experiment by stopping the steam flow and cooling to 250°C in flowing Ar. Shift rate was measured by then saturating 100 sccm of 65% Ar, 35% CO with distilled water at 70°C and passing the gas over the sample. The effluent CO_2 flow rate then equals the net rate of LTWGS. Under these conditions, the reactor was *not* differential, but it was modeled as differential because the relative catalytic activity was all that was needed. The kinetic expression determined by Grenoble *et al.* (*19*) was used to calculate a site-specific rate at these conditions. The ratio of the measured rate to the calculated rate yielded the relative number of sites under these conditions. The site density reported by Iglesia and Boudart (*20*) was then used to convert the number of sites to a surface area of nickel from which an average particle size was also calculated. In this manner, it was possible to measure the surface area changes of a sample without removing it from the reactor.

RESULTS

The effect of the standard 5-min pretreatment (1000 K, 1 atm, 100 sccm dry Ar) used throughout this investigation upon the conversion of both catalyzed and uncatalyzed Spherocarb and graphite was ascertained using the flow reactor. In all cases, a weight loss was measured which corresponded to conversion of less than 4% of the carbon. During the pretreatment, carbon oxides were evolved; however, at the end of the 5-min pretreatment, these gases were released at an apparent gasification rate more than 10 times slower than the rate observed when steam was subsequently added to the reactor feed. Also it was observed that increasing the duration of the pretreatment further reduced the apparent gasification rate measured at the end of the pretreatment but that subsequent reactivity in steam was lessened as well.

Representative steam gasification behavior of 5 wt% Ni-catalyzed graphite is demonstrated by the burnoff of curve plotted in Fig. 1. In that figure, as in subsequent burnoff curves, the integral rate of carbon conversion, calculated from the effluent reactor composition and flow rate, is plotted as a function of the percentage of the carbon gasified. The percentage of the carbon gasified was determined by integration of the observed rate over the time of reaction using the measured change in sample mass for normalization. Figure 1 also includes a time scale for reference. Under the same conditions, the rate of gasification of uncatalyzed graphite is over 100 times smaller

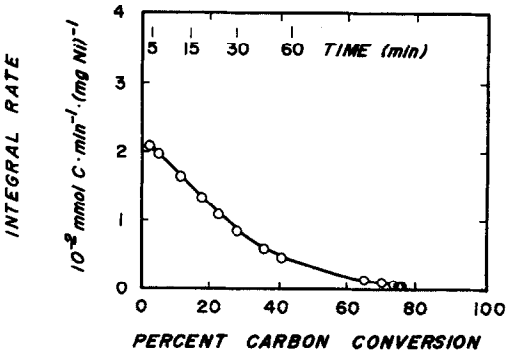

FIG. 1. Burnoff behavior of 5 wt% Ni-catalyzed graphite. Integral rate was determined at 810 K and ca. 0.1 MPa in 125 sccm flow of 20% H_2O in Ar using an initial sample mass of 180.8 mg.

than the rates shown in Fig. 1 (using a hypothetical 5 wt% catalyst loading to allow comparison on an approximately equal basis). The composition of the reactor effluent was observed to more closely approach water-gas sift equilibrium as conversion increased. At 1000 K the carbon conversion was greater than 80% when the integral rate had declined by the same relative amount as that shown in Fig. 1.

In separate experiments the burnoff of a 5 wt% Ni-catalyzed graphite under conditions like those of Fig. 1 was stopped after 5, 15, and 60 min of steam flow. The average nickel particle size of the sample recovered from the reactor in each case was measured by X-ray diffraction (XRD) line broadening of the metallic nickel signal (*21*). In another experiment, it was shown that stopping the reaction, removing the sample, storing overnight, reloading the sample into the reactor, and resuming burnoff did not change the course of the burnoff from that in Fig. 1. The low-temperature (523 K) water-gas shift reaction rate was also used as an *in situ* surface area probe. A single 5 wt% Ni-catalyzed graphite sample was reacted under conditions like those in Fig. 1. However, after 5, 15, and 30 min in steam flow, the LTWGS rate was measured, and the nickel surface was estimated. The sample condition after 5 min in steam was chosen as a reference condition, and the integral rate of steam gasification and the surface area at this point were assigned relative values of 100%. Table 1 presents the changes in these quantities as burnoff progresses.

A nickel-catalyzed single-crystal graphite specimen, mounted on a gold microscopy grid, was steam-gasified under conditions similar to those of Fig. 1 except the temperature was 1000 K. The burnoff was terminated approximately halfway through its course, and the specimen was removed and examined in a scanning transmission electron microscope. Figure 2 is a low-magnification micrograph of the specimen showing an edge region of the graphite single crystal. The edges of the single crystal are the regions where most catalytic attack is expected to occur (*22*), and indeed this is observed. No evidence of channels is found in this particular micrograph.

TABLE 1

Relative Changes in Steam Gasification Rate and Metal Surface Area During Burnoff of 5 wt% Ni-Catalyzed Graphite

Time (min)	Integral steam gasification rate (%)	Nickel surface area	
		by XRD (%)	by LTWGS (%)
5	100[a]	100[b]	100[c]
15	76	104.6	99.4
30	52	n.m.[d]	95
60	28	83	n.m.

[a] 2.1×10^{-2} mmol C/min · mg Ni.
[b] 1.5×10^{-13} m²/g Ni.
[c] 2.2×10^{-16} m²/g Ni.
[d] n.m. = not measured.

The burnoff behavior of 5 wt% Ni-catalyzed Spherocarb was similarly studied. Figure 3 is a plot of the integral rate of steam gasification of 5 wt% Ni-catalyzed Spherocarb as a function of the carbon conversion; as in Fig. 1 an elapsed time scale is also included. The apparent deactivation in the Spherocarb case is greater in magnitude and more abrupt than in the graphite case. The final observed rate is less than 1% of the maximum observed rate. As with the graphite case, initially the uncatalyzed gasification rate is negligible. However, at the end of the run the observed integral steam gasification rate was only 5 to 10 times larger than the rate measured with an equivalent amount of fresh uncatalyzed Spherocarb. Also with 5 wt% Ni-catalyzed Spherocarb the reactor effluent was observed to become less equilibrated with respect to water-gas shift as the burnoff proceeded. The carbon conversion at which the catalyst was fully deactivated was nearly constant at 35 to 40% over the tem-

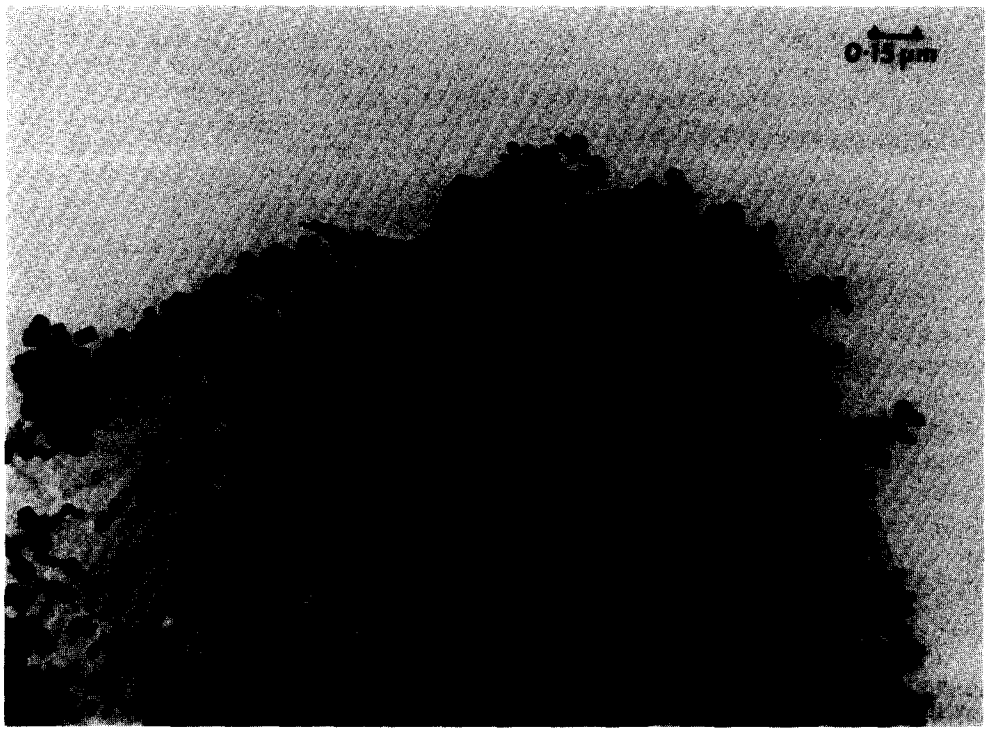

FIG. 2. Transmission electron micrograph of nickel-catalyzed single crystal graphite after steam gasification at 1000 K and ca. 0.1 MPa.

perature range from 723 to 1000 K in agreement with the results reported by Wigmans and Moulijn (*1*).

The nickel surface area and particle size as a function of burnoff in steam at 813 K were also probed. Particle sizes were estimated using XRD line broadening and also

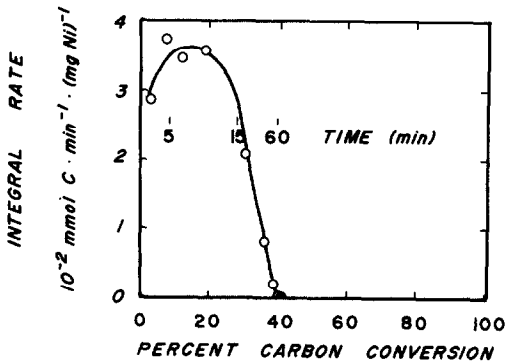

FIG. 3. Burnoff behavior of 5 wt% Ni-catalyzed Spherocarb. Integral rate was determined at 810 K and ca. 0.1 MPa in 125 sccm flow of 20% H_2O in Ar using an initial sample mass of 180.0 mg.

by direct examination of the samples by STEM after the standard pretreatment, 5 min in steam, 15 min in steam, and 60 min in steam. Figure 4 is a micrograph of the sample which only was pretreated while Fig. 5 is a micrograph of a sample after steam gasification for 60 min. For each of the four samples just described, a number of micrographs similar to Figs. 4 and 5 were obtained. From these micrographs particle size distributions were determined by counting between 62 and 283 particles per sample. There were no significant differences in the shapes of the particle size distributions. From the particle size distributions, a number-average particle size was calculated. The resulting particle sizes along with those determined by XRD line broadening are listed in Table 2.

The rate of LTWGS was also used to probe the nickel catalyst surface area *in situ* as with the graphite samples. The apparent surface area measured in this way is plotted

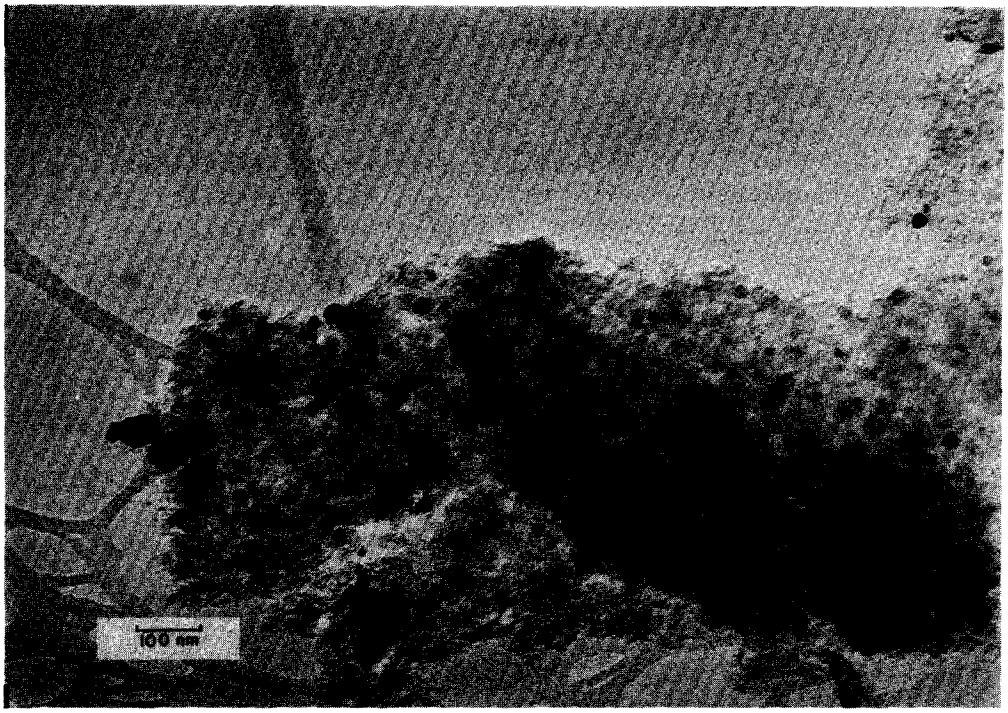

FIG. 4. Transmission electron micrograph of 5 wt% nickel-catalyzed Spherocarb after pretreatment at 1000 K and 0.1 MPa for 5 min in flowing Ar.

FIG. 5. Transmission electron micrograph of (initially) 5 wt% nickel-catalyzed Spherocarb after pretreatment and steam gasification at 813 K for 60 min.

TABLE 2

Nickel Particle Sizes as a Function of Burnoff in Steam at 813 K for 5 wt% Nickel-Catalyzed Spherocarb

Time reacted in steam at 813 K (min)	Average particle size (Å)	
	by STEM	by XRD
0	215	n.m.
5	209	160
15	298	170
60	286	190

against time in the semilogarithmic graph of Fig. 6. Data are shown for gasification in steam at 813 and at 1000 K. The data are adequately fit by an exponential relationship of the form

$$A = A_0 e^{-\alpha t}, \quad (1)$$

where A is the apparent nickel surface area measured by LTWGS, t is the time exposed to steam gasification, and A_0 and α are constants. The constants A_0 and α were determined to be 7.4×10^{19} Å^2/mg Ni and 0.057 min^{-1}, respectively, at 813 K by least-squares fitting. At 1000 K the values were 8.2×10^{19} Å^2/mg Ni and 0.187 min^{-1}, respectively. Chemisorption of CO (during CO_2 gasification—discusssed later) evidenced a significant decrease in metal surface area also.

A series of steam gasification experiments were performed at 1000 K and ca. 0.1 MPa using two consecutive carbon beds within the reactor. Thus, the products of reaction in the first, upstream bed passed immediately into the second, downstream bed which was less than 1 cm below and separated by a small quartz wool plug. In all cases, the second, downstream bed was 5 wt% nickel-catalyzed graphite. Also, in all cases, the first, upstream bed was an uncatalyzed carbon. The results of these experiments are shown in Fig. 7 which shows resultant burnoff curves. The integral rates are normalized by the mass of nickel catalyst in the second, downstream bed, thus assuming that the first upstream bed (being uncatalyzed) makes a negligible contribution to the measured rate. An upstream bed of graphite exerted no significant effect upon the behavior observed in the absence of an upstream bed. Sphero-

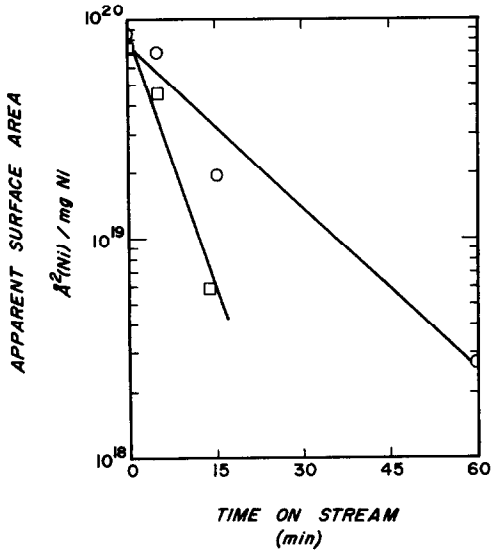

FIG. 6. Decrease in apparent nickel surface area as determined by LTWGS as a function of steam gasification time for 5 wt% nickel-catalyzed Spherocarb (○, 813 K; □, 1000 K).

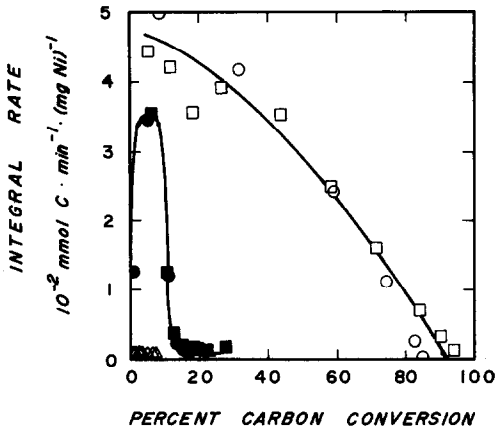

FIG. 7. Dual-bed steam gasification burnoff curves for 1000 K, 0.1 MPa reaction in 125 sccm of 20% H_2O in Ar. In all cases, downstream bed is 5 wt% nickel-catalyzed graphite. Upstream beds are ○, none; □, graphite; ●, Spherocarb; ■, activated charcoal; and △, demineralized Illinois No. 6 coal. In all cases, each bed is ca. 150 mg.

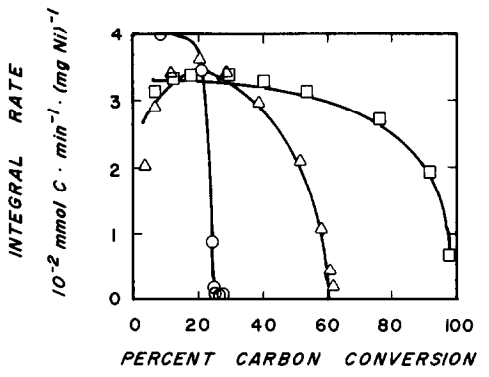

FIG. 8. CO_2 gasification behavior at 1000 K and ca. 0.1 MPa in 120 sccm of 13% CO_2 in Ar. □, 5 wt% Ni-catalyzed graphite; ○, 5 wt% Ni-catalyzed Spherocarb; and △, dual beds of uncatalyzed Spherocarb upstream and 5 wt% Ni-catalyzed graphite downstream.

carb or activated carbon as upstream beds caused rapid catalyst deactivation in the downstream bed, and coal char in the upstream bed eliminated completely the catalytic activity of the downstream bed.

Gasification using CO_2 and H_2 were also examined. The results were very similar to those observed with steam. Figure 8 summarizes the CO_2 gasification behavior. With 5 wt% nickel-catalyzed graphite at 1000 K and ca. 0.1 MPa, the burnoff extends to high limits with only slight indications of deactivation. On Spherocarb the catalyst displays marked deactivation. Significantly, H_2 was detected in the product mixture from this reaction. As observed with steam in dual-bed gasification, an upstream bed of uncatalyzed Spherocarb alters the activity of the catalyst in a downstream 5 wt% nickel catalyzed graphite bed. Figure 9 shows the same phenomena for H_2 gasification, but due to the lower rate of this reaction, the carbon conversion levels are much lower.

DISCUSSION

The results presented in the previous section show that the chemical form of the carbon being catalytically gasified impacts upon the course of nickel catalyst deactivation (compare Figs. 1 and 3). In all cases considered, the uncatalyzed reaction rate was observed to be too small to directly account for the behavior differences. Furthermore, as noted previously, the standard sample pretreatment procedure was demonstrated to be effective in removal of a large fraction of the residual oxygen and hydrogen remaining in or on the samples after preparation and atmospheric handling. In light of their different deactivation behaviors, nickel-catalyzed graphite and Spherocarb will be discussed separately beginning with the graphite system.

The primary reaction during steam gasification may be written as

$$C + H_2O \rightarrow CO + H_2 \qquad (1)$$

However, the products also include CO_2 and CH_4 which might be considered to arise from the secondary reactions

$$CO + H_2O \rightarrow CO_2 + H_2 \qquad (2)$$

and

$$C + 2H_2 \rightarrow CH_4 \qquad (3)$$

Indeed, many other reactions can also be written to describe the observed product mixture, and reactions (1) through (3) are not necessarily the only routes to produce each of the products. A nickel catalyst does accelerate each of these reactions relative to the uncatalyzed situation.

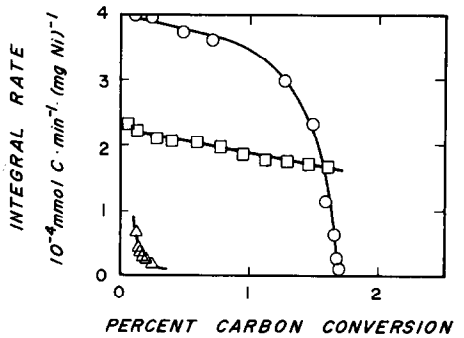

FIG. 9. H_2 gasification behavior at 1000 K and ca. 0.1 MPa in 120 sccm of 13% H_2 in Ar. □, 5 wt% Ni-catalyzed graphite; ○, 5 wt% Ni-catalyzed Spherocarb; and △, dual beds of uncatalyzed Spherocarb upstream and 5 wt% Ni-catalyzed graphite downstream.

A. The Ni/Graphite System

The declining integral gasification rate shown in Fig. 1 is probably primarily a result of catalyst sintering under reaction conditions. The rates plotted in the figure are normalized using the catalyst mass, and consequently, decreases in the metal surface area would cause apparent deactivation. In this study, two methods were utilized to estimate the nickel surface area. The first was XRD line broadening from which a mean crystallite diameter can be calculated. The particle diameters estimated using this technique on steam gasification samples ranged from 210 to 265 Å. These estimates seem quite reasonable. The second method involved measuring the rate of the WGS reaction and calculating a surface area based upon reported kinetic parameters for a similar system. In this case the analysis yielded values ranging from 7.90 to 8.32 Å. These estimates are unreasonably low, most probably because the kinetic parameters are not the same for Ni/C as for Ni/Al_2O_3. Nonetheless, the relative changes in these values will reflect the relative change in particle size provided the reaction is not in a structure sensitive regime. The XRD particle size of greater than 200 Å indicates this is likely. Therefore, the changes indicated in Table 1 should reflect the change in metal surface area. In addition, the surface area measurement using WGS rates is effective in tracking the gasification activity of Ni/Spherocarb as will be discussed later in this section. Table 1 thus indicates that were the integral rates normalized using the metal surface area, the catalyst would still exhibit deactivation.

In the metal-catalyzed gasification reactions one step in the mechanism is often assumed to be the activation of carbon on the metal surface (*23*):

$$C_{bulk} + M \rightarrow M\text{–}C \qquad (4)$$

Once the carbon has been activated, i.e., is present on the metal surface as so-called carbidic carbon (*24*), it then reacts with other adsorbed species, such as oxygen or hydroxyl species resulting in gasification. However, there is a second route for the carbidic carbon, namely, dissolution into the bulk of the metal. This second route remains available as long as the metal is not saturated with carbon. Experiments with graphite-supported iron indicate that in the absence of strongly carburizing gases like acetylene the saturation of the metal may require hours (*25*). The decreasing catalyst activity shown in Fig. 1 may be caused by the increasing carbon content of the metal. Increasing the carbon content of the metal might cause deactivation in several ways. For example, it has been reported that Fe_3C does not wet graphite (*26*). Thus, as the metal becomes more carburized, the interaction between it and the graphite may weaken so that carbon activation [reaction (4)] is reduced. It is important that (i) this deactivation is distinct from that of Ni/Spherocarb and (ii) even at the latest stages the system is 100-fold more active than the uncatalyzed graphite.

The low-magnification micrograph of Fig. 2 evidences another possible explanation for the deactivation of the catalyst during reaction. The individual catalyst particles are seen to cluster together into large aggregates. In this form the nickel surface area is largely unaccessed by the carbon substrate and yet still measurable via XRD or gas-phase probes like WGS. However, before extending this observation to interpret the activity decline shown in Fig. 1, it must be noted that the graphite in the microscope specimens is large single-crystal material in contrast to the kinetic samples which contain much smaller graphite domains. The ratio of basal carbon to edge carbon sites is therefore expected to be smaller in the kinetic samples. Since agglomeration is often observed on the basal surfaces whereas catalytic attack occurs at edges (*22*), the situation in Fig. 2 may be exaggerated.

Finally, with respect to nickel-catalyzed steam gasification of graphite, it has been

observed (*22*) that the reaction rate is dependent upon the catalyst particle diameter, varying in proportion to the inverse square root of the diameter. Using the XRD-determined particle sizes, this effect can only explain a decline in rate of ca. 10%, which is significantly less than the amount in Table 1, even when corrected for the metal surface area.

B. The Ni/Spherocarb System

While the carburization processes discussed above, in conjunction with the graphite system, are likely also operative with Spherocarb, the apparent deactivation of nickel during steam gasification of Spherocarb shown in Fig. 3 is most probably, primarily a result of encapsulation of the metal by an inactive, graphitic carbon overlayer. This situation has been observed during the Pd-catalyzed CO_2 gasification of amorphous carbon (*27*), and many observations from the present study support this hypothesis.

The extent of water-gas shift during steam gasification reaction (2), is consistent with an encapsulation mechanism. Even at 250°C nickel is a very active shift catalyst (*19*). It is not surprising therefore to observe that the shift reaction is close to equilibrium throughout the course of nickel-catalyzed steam gasification of SP-1 graphite. In that case, the approach to equilibrium increases throughout the burnoff as previously noted. This would be expected since the steam gasification rate decreases and thus the amount of CO produced decreases. A decreased CO content requires fewer shift turnovers to attain shift equilibrium, or conversely at a fixed rate of shift a decreased CO content allows a closer approach to equilibrium. When nickel-catalyzed Spherocarb is gasified, the shift reaction falls away from equilibrium at the same time the catalyst deactivates for gasification. This provides evidence that the metal surface is no longer available to the gas phase, because as already stated, at lower gasification rates the CO production is low and hence only a small water-gas shift rate is necessary for the system to approach equilibrium. The water-gas shift data are therefore consistent with a nickel encapsulation mechanism. (It should be noted that the shift reaction presently being discussed is that which occurs simultaneously during steam gasification, i.e., reaction (2), and not the LTWGS which has been used in this study as a surface area probe.)

By conducting the steam gasification reaction at 810 K, it was possible to stop the reaction at preselected stages of deactivation. After 5 min on stream, the reactivity of the 5 wt% Ni on Spherocarb was near its maximum; after 15 min on stream the sample was approximately half as active; and after 60 min on stream deactivation was complete. These exposure times thus made suitable samples for studying the catalyst deactivation.

After 60 min on stream the measured reaction rate was greater than the rate measured for fresh uncatalyzed Spherocarb by a factor of 5 to 10. The sample of deactivated catalyzed material may have had a different structure which accounts for this difference. For example, while the catalyst was active, the catalytic reaction may have opened the pore structure creating more accessible reaction sites for the uncatalyzed reaction. Also, not all the catalyst might have been deactivated, but some fraction may have remained active after 60 min. In short, it is not possible to discern whether the catalyst was totally inactive after 60 min or not, but it is certain that the rate had declined by a factor of over 100 from its most active state.

In the case of encapsulation, techniques which directly probe particle size or volume (e.g., STEM and XRD) should not indicate significant changes in these quantities during the course of the deactivation. In contrast, techniques which probe the metal surface directly (chemisorportion, catalytic kinetics, etc.) should indicate massive apparent surface area changes.

The standard pretreatment for 5 min at 1000 K in Ar was sufficient to sinter the catalyst to an average size of ca. 215 Å as determined from the transmission electron micrograph shown in Fig. 4. Generally, the catalyst particles appear round with no distinct features. Examination of a number of areas on this specimen did not indicate any significant differences from Fig. 4. The sample which had been gasified for 60 min (Fig. 5), indicates that the particle size did, indeed, increase during the reaction. However, the changes observed could not be responsible for the rate decline shown in Fig. 3 based solely upon sintering.

X-ray diffraction line broadening was also used to estimate the nickel particle size of samples prepared the same way the STEM samples were prepared. The results of STEM and XRD analyses are listed in Table 2. The mean particle sizes from XRD are approximately 25% smaller than the estimates from the electron micrographs. This agreement is satisfactory for the present purposes. More importantly, the change in particle size reported in Table 2 would result in a metal surface area decrease of only 15%. Thus, the XRD and STEM provide a consistent indication that sintering is not responsible for the deactivation experienced during gasification.

The rate of the low-temperature water-gas shift was again used to probe the available metal surface area. The apparent surface area as a function of time on stream is shown in Fig. 6. The actual value of the area expressed in Fig. 6 is probably not accurate as already discussed. However, the change in the apparent surface area is the desired information, and this can be ascertained with relative certainty from the figure. Clearly, the apparent surface area declines roughly in proportion to the extent of deactivation. Indeed, when the rate is normalized using the apparent nickel surface area, catalyst deactivation is not indicated.

Monolayer graphite phases have been detected on single-crystal nickel surfaces after various carburization treatments (*28, 29*). The graphite monolayer which forms epitaxially on the Ni (111) surface is reported to involve stronger carbon bonding than bulk graphite (*28*). This would explain how a carbon layer could prevent carbon gasification. Once this graphite monolayer forms, there is no metal surface available for catalysis and hence the uncatalyzed reaction would have to react away the layer in order to regain activity. However, the uncatalyzed reaction of graphite at these temperatures is extremely slow, and consequently, if a graphite monolayer did form, it might survive reaction conditions, thereby permanently deactivating the catalyst upon which it formed. In addition, it has been reported that other surfaces of nickel will reconstruct to a (111) surface upon formation of the graphite monolayer. The electron micrographs of the present study are interesting in this regard. In the fresh (i.e., only pretreated) sample (Fig. 4), the nickel particles appear featureless. However, in Fig. 5, a steam-gasified sample, many of the metal particles appear to possess regular, facetted shapes. Also when nickel is supported on basal plane graphite, the metal particles exhibit these shapes as seen in Fig. 2. One possibility is that these regular shapes result from the same forces responsible for the epitaxial growth of graphite monolayers on Ni(111) surfaces.

The source of the proposed encapsulating overlayer is suggested to be a gas-phase species by the results of dual-bed gasification (Fig. 7). Specifically, Fig. 7 shows that the nickel catalyst on an SP-1 graphite substrate can be made to deactivate during steam gasification simply by passing the reactant steam through a bed of uncatalyzed Spherocarb at reaction conditions before it contacts the catalyzed graphite. An upstream bed of SP-1 graphite has no effect. Spherocarb is not unique in this regard; activated coconut charcoal has the same effect, and Illinois coal char is even worse.

The material causing the deactivation has not been detected but is believed to be a hydrocarbon present as part of the carbon

structure. The concentration of this species is apparently very small at the reactor outlet. This would explain the detection of H_2 in the products during CO_2 gasification. The hydrocarbon may catalytically decompose upon the metal surface generating H_2 and surface carbidic carbon, and the surface carbidic carbon can condense producing a graphitic overlayer, as previously discussed (*28, 29*). Spherocarb does contain both hydrogen and oxygen (*16*), and it is essentially free of traditional catalyst poisons like sulfur.

Finally, though not emphasized in this report, CO_2 and H_2 gasification proceed similarly to H_2O with respect to deactivation. Figures 8 and 9 indicate that similar phenomena occur with these gases, and deactivation can be attributed to a common cause. As a caution, it should be noted that hydrogen reduction of a carbon-supported nickel catalyst could result in metal decoration or encapsulation and anomalous chemisorptive and kinetic results.

CONCLUSIONS

Nickel catalyst deactivation during steam gasification of carbon has been demonstrated to differ depending upon the chemical nature of the carbon. When high-purity graphite is gasified, a moderate deactivation is observed which cannot be attributed to sintering or particle size effects. A model catalyst/single-crystal graphite system exhibited nickel particle clustering which could explain the deactivation, but this phenomenon has not yet been demonstrated on real systems. Carburization of the nickel is also possibly responsible for catalyst deactivation.

When less-ordered carbon structures, which also contain hydrogen and oxygen, are steam-gasified, the nickel catalysts undergo more severe and rapid deactivation. Particle size increases only slightly during this process, whereas apparent metal surface area decreases significantly. Encapsulation of the nickel particles by an epitaxial carbon layer is consistent with observed behavior. Dual-bed gasification experiments indicate that the proposed carbon overlayer arises from the decomposition of a hydrocarbon species released during reaction.

Similar conclusions are indicated in the cases of CO_2 and H_2 gasification. In addition to obvious implications in catalytic coal gasification, the findings suggest caution in other processes. Decoking of nickel catalysts with steam or hydrogen under appropriate conditions might lead to catalyst encapsulation. Also carbon-supported nickel catalysts subjected to high-temperature reduction could be subject to similar results.

ACKNOWLEDGMENTS

The experimental work which was performed by Peter Kudyba and Rexford Sherwood, Exxon, is gratefully acknowledged. Dr. R. Liotta, Exxon, provided the deashed, demineralized coal sample. Finally, fruitful discussions with Dr. D. J. Doonan and Dr. R. T. K. Baker, Exxon, are appreciated and acknowledged.

REFERENCES

1. Wigmans, T., and Moulijn, J. A., *in* "New Horizons in Catalysis" (T. Seiyama and K. Tanabe, Eds.), Vol. 7A, p. 501. Elsevier Scientific, New York, 1981.
2. Euker, C. A., Jr., and Wesselhoft, R. D., *Energy Prog.* **1,** 12 (1981).
3. Rostrup-Nielson, J. R., "Steam Reforming Catalysts." Teknish Forlag, Copenhagen, 1975.
4. Yan, T. Y., and Rosynek, M. P., *ACS Div. Pet. Chem., Prepr.* **24,** 780 (1979).
5. Holstein, W. L., *Fuel* **62,** 259 (1983).
6. McKee, D. W., *AIP Conf. Proc.* (Chem. Phys. Coal Util.-1980) **70,** 236 (1981).
7. McKee, D. W., *Chem. Phys. Carbon* **16,** 1 (1981).
8. Colle, K. S., Kim, K., and Wold, A., *Fuel* **62,** 155 (1983).
9. Kim, K., Kershaw, R., Dwight, K., Wold, A., and Colle, K., *Mater. Res. Bull.* **17,** 591 (1982).
10. Wigmans, T., van Dam, F., and Moulijn, J. A., *Carbon* **19,** 309 (1981).
11. Wigmans, T., van Doorn, J., and Moulijn, J. A., *Ext. Abstr. Program–Bienn. Conf. Carbon 16th,* 172 (1983).
12. McKee, D. W., *Carbon* **12,** 453 (1974).
13. Tamai, Y., Watanbe, H., and Tomita, A., *Carbon* **15,** 103 (1977).
14. Tomita, A., Higashiyama, K., and Tamai, Y., *Fuel* **60,** 103 (1981).
15. Tomita, A., and Tamai, Y., *Fuel* **60,** 992 (1981).

16. Ebert, L. B., Mills, D. R., and Scanlon, J. C., *Mater. Res. Bull.* **17,** 1319 (1982).
17. Baker, R. T. K., *Catal. Rev.-Sci. Eng.* **19,** 161 (1979).
18. Kay, D. H., "Techniques for Electron Microscopy." Blackwell, Oxford, 1965.
19. Grenoble, D. C., Estadt, M. M., and Ollis, D. F., *J. Catal.* **67,** 90 (1981).
20. Iglesia, E., and Boudart, M., *J. Catal.* **81,** 204 (1983).
21. Klug, H. P., and Alexander, L. E., "X-Ray Diffraction Procedures for Polycrystalline and Amorphous Materials," 2nd ed. Wiley, New York, 1974.
22. Baker, R. T. K., and Sherwood, R. D., *J. Catal.* **70,** 198 (1981).
23. Holstein, W. L., and Boudart, M., *J. Catal.* **75,** 337 (1982).
24. McCarty, J. G., Hou, P. Y., Sheridan, D., and Wise, H., *ACS Symp. Ser.* **202,** 253 (1982).
25. Baker, R. T. K., and Sherwood, R. D., *J. Catal.*, in press.
26. Humenik, M., Hall, D. W., and van Alsten, R. L., *Met. Prog.* **4,** 101 (1962).
27. Holstein, W. L., Moorhead, R. D., Poppa, H., and Boudart, M., *Chem. Phys. Carbon* **18,** 139 (1982).
28. Shelton, J. C., Patil, H. R., and Blakely, J. M., *Surf. Sci.* **43,** 493 (1974).
29. Eizenberg, M., and Blakely, J. M., *J. Chem. Phys.* **71,** 3467 (1979).